Shape Transformations of Vesicles Induced by Swim Pressure

Yao Li* and Pieter Rein ten Wolde†
AMOLF, Science Park 104, 1098 XG Amsterdam, Netherlands

(Received 21 February 2019; published 30 September 2019)

While the behavior of vesicles in thermodynamic equilibrium has been studied extensively, how active forces control vesicle shape transformations is not understood. Here, we combine theory and simulations to study the shape behavior of vesicles containing active Brownian particles. We show that the combination of active forces, dimensionality, and membrane bending free energy creates a plethora of novel phase transitions. At low swim pressure, the vesicle exhibits a discontinuous transition from a spherical to a prolate shape, which has no counterpart in two dimensions. At high swim pressure it exhibits stochastic spatiotemporal oscillations. Our work helps researchers to understand and control the shape dynamics of membranes in active-matter systems.

DOI: 10.1103/PhysRevLett.123.148003

Active matter systems containing self-propelled units are not only omnipresent in the natural world [1–3], but are also increasingly made synthetically [4–9]. These systems are inherently out of thermodynamic equilibrium and show behavior that cannot be observed in equilibrium systems, such as spontaneous flow [10–13], athermal phase separation [14–16], or oscillations [17]. A key quantity in these active systems is the swim pressure [18–20], which in contrast to the thermodynamic pressure depends on the shape of the boundary [21–23]. In both natural and synthetic systems, boundaries are often formed by soft lipid bilayers, which can change shape under the influence of pressure. Yet, the feedback between swim pressure and membrane shape dynamics is not understood.

Here we study shape transformations of vesicles containing active particles. Passive vesicles in thermodynamic equilibrium exhibit a variety of shapes, including prolate, oblate, and chain of "pearls" [24,25]. These shapes are governed by the Helfrich bending free energy [26], the osmotic pressure, and, if applicable, the adsorption of particles onto the membrane [25]. How active forces affect vesicle shape is, however, a wide open question [27]. While the osmotic pressure controls vesicle shape only indirectly by setting the volume [24], the swim pressure as generated by active Brownian particles [18–20] also depends on the shape of the membrane [21–23]. Computational studies on active particles confined within a semiflexible ring polymer in 2D show that active forces can change the shape of the polymer from circular to elliptical [28,29], suggesting that the swim pressure can, unlike the osmotic pressure, also directly control vesicle shape. Yet how the swim pressure interacts with membrane elasticity to control shape, and how this interaction depends on the dimensionality of the system, are not understood. Here we show that this interaction is fundamentally different in 2D and 3D and that as a result 3D vesicles exhibit shape transformations not observed in 2D. At low swim pressure, the vesicle exhibits a discontinuous transition from a spherical to a prolate shape, while at high swim pressure it shows exotic spatiotemporal oscillations which we call active vesicle pearling.

In our model the active Brownian particles have a self-propulsion velocity v_0 and interact with each other and with the membrane of the vesicle via a short-ranged repulsive potential [30]. The membrane is described by a Helfrich bending free energy [26], augmented by two terms that allow us to control the membrane area and the reduced volume $\hat{V}$, which is the volume of the vesicle relative to that of a sphere with the same area [30]. Since lipid membranes are typically impermeable for colloidal particles and proteins of 10–100 nm in diameter, we keep the number of particles within the vesicle fixed.

Figure 1(a) shows that active forces can drastically affect the shape behavior of vesicles. The figure shows the phase diagram as a function of the self-propulsion speed v_0 and the reduced volume $\hat{V}$, which can be controlled experimentally via the osmotic pressure [44]. When the self-propulsion speed v_0 is zero, the system reproduces the phase behavior of vesicles in thermodynamic equilibrium [24]: as the reduced volume $\hat{V}$ is decreased, the vesicle exhibits a series of shape transformations, from spherical to prolate, oblate, and eventually to a stomatocyte. However, our results show that when the system is driven out of thermodynamic equilibrium, by increasing v_0, the stomatocyte and the oblate shape loose their stability, while the prolate shape is favored. This is due to a positive feedback between the accumulation of particles in curved regions of the membrane and the higher pressure that these particles generate, which increases the curvature. This mechanism drives the vesicle to a prolate shape in which the particles accumulate at the poles of the vesicle.

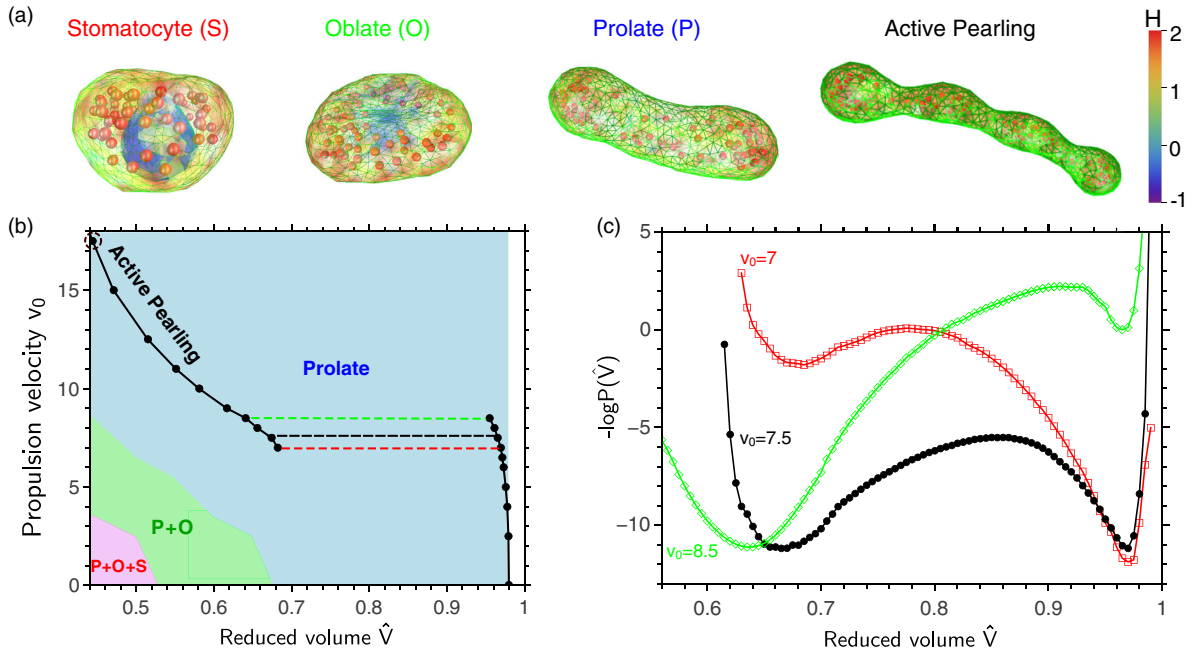

FIG. 1. Shape transformations of a vesicle containing active particles. (a) Vesicle shapes that arise from the interplay between the membrane elastic bending energy and the swim pressure. The active particles are in red, the triangular membrane mesh in green, and the local membrane mean curvature H color coded. Shape order parameters are described in Ref. [30]. (b) Phase diagram as a function of the self-propulsion speed v_0 and the reduced volume $\hat{V}$. Blue region represents parameter sets for which only the prolate (P) shape is (meta) stable; the green and red regions denote parameter combinations for which, respectively, prolate and oblate (O) shapes, and prolate, oblate, and stomatocyte (S) shapes, are (meta) stable; a state was considered (meta)stable if it persisted for at least 100 s. Note that the prolate shape becomes more stable at higher v_0. Superimposed on the phase diagram with black lines is the "equation of state" $\hat{V}(v_0)$ for vesicles in which the osmotic pressure is zero, which allows the volume to change freely. Between $v_0 \approx 7$ μm/s and $v_0 \approx 8.5$ μm/s the vesicle exhibits a discontinuous transition from a fairly spherical to a distinctly prolate shape. In this range, the two states are separated by a generalized free-energy barrier, see panel (c). For higher values of v_0, the system exhibits active pearling, see also Fig. 4(c). Generalized free energy $-\log P(\hat{V})$ as a function of the reduced volume $\hat{V}$ for three values of v_0, corresponding to the dashed lines in panel (a). The panel shows that at $v_0 = 7.5$ μm/s the two states are equally stable while at $v_0 = 7$ μm/s and $v_0 = 8.5$ μm/s the spherical and prolate shape are about to loose their stability, respectively. The bending rigidity of the vesicle is $\kappa = 30 k_B T$ and its surface area $A_0 = 4\pi R_0^2$, with $R_0 = 1$ μm. The particle diameter $\sigma = 0.2$ μm and the particle number $N = 60$; this means that the volume fraction for the particles in a spherical vesicle is $\varphi \approx 5\%$. The particles' rotational diffusion constant is $D_r = 1$ s^{-1}, and the translational diffusion constant of the particles D_t and that of the nodes of the membrane mesh, D_m, is $D_t = D_m = 0.1$ μm^2/s.

Clearly, active forces can quantitatively change the shape behavior of vesicles when their volume is controlled. However, in many experimental systems the osmotic pressure is zero, which means that the volume is free to change [44]. The lines connecting the blacks dots in Fig. 1(a) show that in this scenario a new, discontinuous phase transition arises. These lines show the "equation of state," the relation between the reduced volume $\hat{V}$ and the propulsion velocity v_0. As expected, $\hat{V}$ decreases as v_0 is increased. Particles with higher propulsion velocity generate a higher force at the two poles of the vesicle, stretching the vesicle and reducing its volume. Surprisingly, however, the equation of state splits into two branches via a discontinuous transition. One corresponds to a shape that is still fairly spherical, while the other corresponds to a distinct prolate shape. To determine the "coexistence" velocity v_0^{coex} where both shapes are equally likely, we computed as described in Ref. [30] the stationary probability distribution of the reduced volume $P(\hat{V})$ using Forward Flux Sampling (FFS), which is a numerical technique to efficiently simulate rare events in both equilibrium and nonequilibrium systems [31,32]. Figure 1(b) shows the generalized free energy $-\log P(\hat{V})$ as a function of $\hat{V}$ for three different values of v_0. At $v_0 = 7.5$ μm/s, the prolate and spherical shapes are equally stable, yet separated by a barrier, explaining the discontinuous nature of the transition between them. At $v_0 = 7$ μm/s and $v_0 = 8.5$ μm/s, the prolate and spherical shapes are about to loose their stability, respectively.

This discontinuous transition between a symmetrical (circular) and nonsymmetrical (elliptical) shape has not been observed in 2D systems in which active particles are confined within a semiflexible ring polymer [28,29]. Since we expect that the nature of the transition depends on the competition between the elastic and the swim pressure, we analyzed these for the systems in 2D and 3D. Both in 3D [Fig. 2(a)] and 2D [Fig. 2(b)] the elastic pressure increases

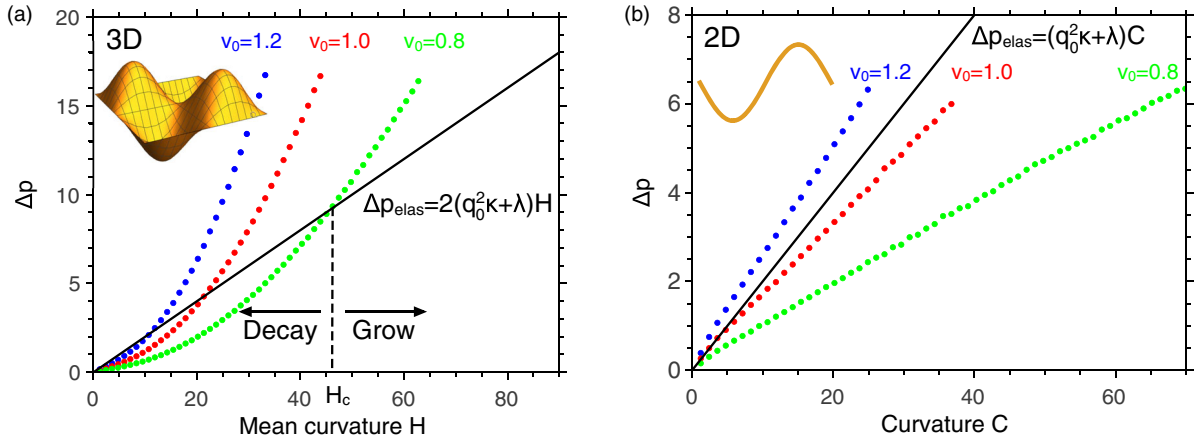

FIG. 2. The nature of the symmetry-breaking transition, discontinuous or continuous, is determined by how the swim and bending pressure depend on curvature. (a) The swim-pressure difference Δp_{swim} for ideal active particles between the outer and inner apices of a sinusoidal surface in 3D as a function of the absolute local mean curvature H at the apices, for three different values of the self-propulsion velocity v_0. Shown also is the elastic pressure Δp_{elas} (black solid line). (b) The swim-pressure difference between the outer and inner apices for a sinusoidal line in 2D as a function of the absolute curvature C, together with the elastic pressure Δp_{elas} (black solid line). While the elastic pressure scales linearly with curvature in both dimensions, the swim pressure scales superlinearly in 3D but weakly sublinearly in 2D. As a result, the sphere-prolate transition in 3D is discontinuous while the corresponding circle-ellipse transition in 2D is continuous. For nonideal particles the swim pressure at high curvature is bounded by their finite size. For parameter values, see Fig. 1.

linearly with the mean curvature [30], suggesting that the different behavior in 2D and 3D is due to the swim pressure.

To elucidate the origin of the scaling behavior of the swim pressure with membrane curvature, we turn to a minimal model system consisting of ideal active particles that do not interact with each other, but do interact with a curved yet static surface. The active particles are confined between two sinusoidal surfaces described by $z_w(x,y) = z_0 + B\sin(2\pi x/L)\sin(2\pi y/L)$ and $-z_w(x,y)$, respectively, where z_0 is chosen to be large enough such that the correlation between the particle distributions at the two respective surfaces vanishes. The local swim pressure per unit density of the active particles $p_{\mathrm{swim}}(x,y)$ is computed by simulations as described in Ref. [30].

The pressure reaches its highest value p_{max} at the outer apices where the particles accumulate, and its lowest p_{min} at the inner apices. Figure 2(a) shows the pressure difference $\Delta p_{\mathrm{swim}} = p_{\mathrm{max}} - p_{\mathrm{min}}$ as a function of the absolute local mean curvature $H = B(2\pi/L)^2$ at the apices. For comparison, we also compute Δp_{swim} in a 2D system with $z_w(x) = z_0 + B\sin(2\pi x/L)$ as in Nikola *et al.* [22], see Fig. 2(b). Surprisingly, while Δp_{swim} grows (sub)-linearly with curvature in 2D, it grows super-linearly in 3D (Fig. 2). The latter observation is consistent with the finding of Fily *et al.* that the density of particles confined to the surface of an ellipsoid is proportional to the local Gaussian curvature [45,46]. The reason why the swim pressure increases superlinearly in 3D and (sub)linearly in 2D is that in 3D there is one more dimension in which the membrane is curved, such that in 3D the particles accumulate more strongly with curvature. This mechanism does indeed not rely on excluded-volume interactions. In fact, given the low particle volume fraction of about 5% at the onset of the sphere-prolate transition, they do not significantly change the scaling behavior (Fig. S1 [30]).

The different scaling of the swim pressure with curvature in 2D and 3D is key to understanding why 3D systems exhibit a discontinuous transition from a symmetrical to a nonsymmetrical shape, while 2D systems do not. Because in 3D the swim pressure varies superlinearly with mean curvature H while the elastic pressure scales linearly with H, there exists a range of v_0 values in which the swim pressure is smaller than the elastic pressure when the curvature H is below a critical value H_c and larger than the elastic pressure when $H > H_c$ [see Fig. 2(b)]. Hence, when the local mean curvature H of a vesicle shape fluctuation is smaller than H_c, the fluctuation tends to decay, while when $H > H_c$ it tends to grow. In this range of v_0 values, a shape fluctuation thus needs to exceed a critical size H_c before it will spontaneously grow further. This explains why there is a barrier for the formation of a curved region of macroscopic size and why the transition from the spherical to the prolate shape is discontinuous. In contrast, in 2D, the near linear dependence of the swim pressure on the curvature means that, depending on the value of v_0, the swim pressure is either larger than the elastic pressure for (almost) all curvature values, or smaller. It is the reason why in 2D the transition from the circular to the elliptical state is continuous.

The above analysis indicates that the barrier arises from the interplay between the dependence of the elastic pressure

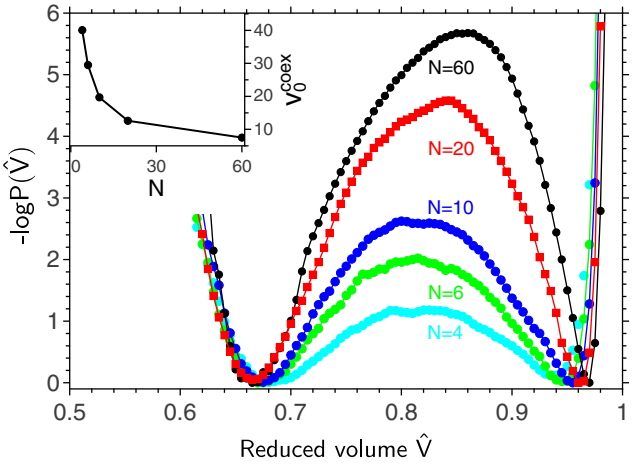

FIG. 3. The self-propulsion velocity and barrier height at sphere-prolate coexistence depend on the number of active particles. Generalized free energy $-\log P(\hat{V})$ as a function of the reduced volume $\hat{V}$ for different number of particles N, with in the inset the coexistence velocity v_0^{coex} as a function of N. While v_0^{coex} decreases with N, the barrier height increases, although both plateau for large N. Other parameter values as in Fig. 1; only the membrane area, and not the volume, is constrained.

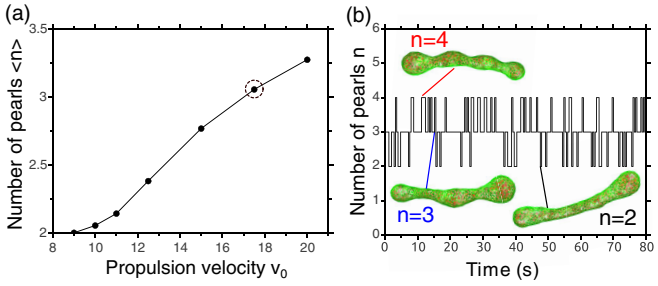

FIG. 4. Active vesicle pearling for high self-propulsion speeds. (a) The average number of pearls increases with the self-propulsion velocity v_0. (b) The number of pearls as a function of time for $v_0 = 17.5\ \mu$m/s, corresponding to the encircled point in panel (a) and Fig. 1(a), with typical snapshots below. The clusters are highly dynamic, see also Supplemental Movie S1 [30]. The membrane area, but not the vesicle volume, is constrained.

and the swim pressure on the curvature, respectively. Since the swim pressure depends on the number of particles N and the translational diffusion constant D_t, we hypothesized that these parameters will affect the height of the barrier. Figure 3 shows that when N is increased, keeping the area of the vesicle constant, the coexistence propulsion velocity v_0^{coex} at which the prolate and spherical shapes are equally likely decreases, while the height of the barrier increases. Increasing N tends to increase the total force that the active particles exert on the membrane. To compensate for this and remain at coexistence, the active force per particle—the propulsion force f_{prop}—must decrease, which is indeed accomplished by lowering v_0: $f_{\mathrm{prop}} = v_0 k_B T / D_t$ (see [30]). Since the force per particle is lower for lower v_0^{coex}, more particles must participate in generating the force to nucleate the shape transformation. This makes the transition more collective and increases the height of the barrier. Figure S1 shows that the height of the barrier also increases with the translational diffusion constant D_t, which can be explained using similar arguments (see Ref. [30]).

When the propulsion velocity v_0 is increased sufficiently beyond the sphere-prolate coexistence region [Fig. 1(a)], the shape dynamics become even richer. More than two clusters are typically formed, with the average number of clusters increasing with v_0 [Fig. 4(a)]. Moreover, these clusters are highly dynamic: Fig. 4(b) shows that they fluctuate in number, while Supplemental Movies S1 and S2 [30] show how they emerge, vanish, and move along the vesicle, splitting into smaller clusters, and merging into larger ones. We call this behavior *active vesicle pearling*.

The clusters form via the interplay between the vesicle shape, the swim pressure, and the interaction between the particles. Indeed, while both finite-sized and ideal particles exhibit a discontinuous sphere-prolate transition because that arises from the feedback between the swim pressure and membrane bending (Figs. 2 and S1), active pearling requires excluded-volume interactions between the particles. Increasing the velocity, active Brownian particles with excluded-volume interactions tend to form dynamic clusters even without confinement [14,15,47]. Additionally, during the elongation of the vesicle not only the density of particles increases as the volume decreases, but also the confining volume is transformed into a quasi-1D tubular shape. Both of these enhance the tendency of the particles to bump into each other and jam to form clusters. Furthermore, while clusters expand the vesicle, the concomitant increase in area must, because of the area constraint, be compensated for by making the necks thinner; the thin necks, in turn, stabilize the clusters further. This dynamic mechanism is further enhanced by the fact that an elongated vesicle in 3D has an intrinsic tendency to form a dumbbell-like shape because that minimizes the Helfrich free energy [24]. Both the latter mechanism and the fact that the vesicle can reduce membrane area by forming a thin neck are absent in 2D, explaining why active pearling is observed in 3D and not in 2D. Clearly, while the phenomenological behavior of active vesicle pearling bears similarities to that of a Rayleigh instability [48], the physical driving forces are different.

For higher D_t and larger system size (increasing both N and vesicle size), the active pearling behavior becomes more pronounced, with clusters moving in an oscillatory yet stochastic fashion from pole to pole. Color coding the different clusters reveals that new clusters tend to be nucleated from the clusters at the vesicle poles (Supplemental Movies S3 and S4 [30]). Only collectively can the particles generate enough force to deform the thin

neck and create a new pearl. The barrier to nucleate a new pearl increases with N and D_t (see Fig. 3 and Fig. S1 [30]), explaining why increasing these parameters makes active pearling more prominent.

In conclusion, our results show how the interplay between active forces and elastic bending forces yields phase behavior that cannot be observed in equilibrium systems [10–17,27]. Our work paves the way for understanding the interplay between active forces and vesicle shape deformations. This could be used in controlling the deformations of synthetic vesicles for, e.g., drug delivery. Our work may also contribute to our understanding of shape transformations of living cells, which are influenced by active forces as generated by, e.g., microtubule filaments. Our predictions can be tested experimentally via vesicles containing Pt-coated colloids or bacteria [49]. We expect that the mechanical torque on the particles as exerted by the membrane and the torque between particles as arising from mechanical or hydrodynamic interactions, which all tend to align particles, will make the transition more collective and hence raise the barrier; the effect of hydrodynamic interactions between the particles and the membrane is more difficult to predict, and requires future work [50,51]. Other fruitful extensions would be the investigation of active particles in vesicles with an active, gel-like cortex or vesicles immersed in a bath of active particles.

This work was supported by the Netherlands Organisation for Scientific Research (NWO). We thank Martin van Hecke, Peter Bolhuis, and Bela Mulder for a critical reading of the manuscript.

*Y.Li@amolf.nl
†tenwolde@amolf.nl

[1] A. Cavagna, D. Conti, C. Creato, L. Del Castello, I. Giardina, T. S. Grigera, S. Melillo, L. Parisi, and M. Viale, Nat. Phys. **13**, 914 (2017).
[2] D. B. Kearns, Nat. Rev. Microbiol. **8**, 634 (2010).
[3] T. Mora, A. M. Walczak, L. Del Castello, F. Ginelli, S. Melillo, L. Parisi, M. Viale, A. Cavagna, and I. Giardina, Nat. Phys. **12**, 1153 (2016).
[4] J. R. Howse, R. A. L. Jones, A. J. Ryan, T. Gough, R. Vafabakhsh, and R. Golestanian, Phys. Rev. Lett. **99**, 048102 (2007).
[5] H.-R. Jiang, N. Yoshinaga, and M. Sano, Phys. Rev. Lett. **105**, 268302 (2010).
[6] D. A. Wilson, R. J. M. Nolte, and J. C. M. van Hest, Nat. Chem. **4**, 268 (2012).
[7] J. Palacci, S. Sacanna, A. P. Steinberg, D. J. Pine, and P. M. Chaikin, Science **339**, 936 (2013).
[8] A. Bricard, J. B. Caussin, N. Desreumaux, O. Dauchot, and D. Bartolo, Nature (London) **503**, 95 (2013).
[9] D. Needleman and Z. Dogic, Nat. Rev. Mater. **2**, 17048 (2017).
[10] R. Voituriez, J. F. Joanny, and J. Prost, Phys. Rev. Lett. **96**, 028102 (2006).
[11] P. Galajda, J. Keymer, P. Chaikin, and R. Austin, J. Bacteriol. **189**, 8704 (2007).
[12] M. B. Wan, C. J. Olson Reichhardt, Z. Nussinov, and C. Reichhardt, Phys. Rev. Lett. **101**, 018102 (2008).
[13] A. Doostmohammadi, J. Ignés-Mullol, J. M. Yeomans, and F. Sagués, Nat. Commun. **9**, 3246 (2018).
[14] J. Tailleur and M. E. Cates, Phys. Rev. Lett. **100**, 218103 (2008).
[15] G. S. Redner, M. F. Hagan, and A. Baskaran, Phys. Rev. Lett. **110**, 055701 (2013).
[16] I. Buttinoni, J. Bialké, F. Kümmel, H. Löwen, C. Bechinger, and T. Speck, Phys. Rev. Lett. **110**, 238301 (2013).
[17] F. C. Keber, E. Loiseau, T. Sanchez, S. J. DeCamp, L. Giomi, M. J. Bowick, M. C. Marchetti, Z. Dogic, and a. R. Bausch, Science **345**, 1135 (2014).
[18] S. C. Takatori, W. Yan, and J. F. Brady, Phys. Rev. Lett. **113**, 028103 (2014).
[19] X. Yang, M. L. Manning, and M. C. Marchetti, Soft Matter **10**, 6477 (2014).
[20] A. P. Solon, J. Stenhammar, R. Wittkowski, M. Kardar, Y. Kafri, M. E. Cates, and J. Tailleur, Phys. Rev. Lett. **114**, 198301 (2015).
[21] A. P. Solon, Y. Fily, A. Baskaran, M. E. Cates, Y. Kafri, M. Kardar, and J. Tailleur, Nat. Phys. **11**, 673 (2015).
[22] N. Nikola, A. P. Solon, Y. Kafri, M. Kardar, J. Tailleur, and R. Voituriez, Phys. Rev. Lett. **117**, 098001 (2016).
[23] G. Junot, G. Briand, R. Ledesma-Alonso, and O. Dauchot, Phys. Rev. Lett. **119**, 028002 (2017).
[24] U. Seifert, Adv. Phys. **46**, 13 (1997).
[25] Y. Yu and S. Granick, J. Am. Chem. Soc. **131**, 14158 (2009).
[26] W. Helfrich, Z. Naturforsch. C **28**, 693 (1973).
[27] A. Mietke, F. Jülicher, and I. F. Sbalzarini, Proc. Natl. Acad. Sci. U.S.A. **116**, 29 (2019).
[28] W.-d. Tian, Y.-k. Guo, K. Chen, and Y.-q. Ma, Chin. Phys. B **26**, 100502 (2017).
[29] M. Paoluzzi, R. Di Leonardo, M. C. Marchetti, and L. Angelani, Sci. Rep. **6**, 34146 (2016).
[30] See Supplemental Material at http://link.aps.org/supplemental/10.1103/PhysRevLett.123.148003 for details of model and methods, additional numerical simulations, and four supplemental movies, which includes Refs. [18,22,26,31–43].
[31] R. J. Allen, P. B. Warren, and P. R. ten Wolde, Phys. Rev. Lett. **94**, 018104 (2005).
[32] C. Valeriani, R. J. Allen, M. J. Morelli, D. Frenkel, and P. R. ten Wolde, J. Chem. Phys. **127**, 114109 (2007).
[33] G. Gompper and D. M. Kroll, in *Statistical Mechanics of Membranes and Surfaces*, edited by D. R. Nelson, S. Weinberg, and T. Piran, 2nd ed. (World Scientific, Singapore, 2002).
[34] H. Noguchi and G. Gompper, Phys. Rev. E **72**, 011901 (2005).
[35] Z.-c. Ou-Yang and W. Helfrich, Phys. Rev. Lett. **59**, 2486 (1987).
[36] R. Dimova, Adv. Colloid Interface Sci. **208**, 225 (2014).
[37] C. Bechinger, R. Di Leonardo, H. Löwen, C. Reichhardt, G. Volpe, and G. Volpe, Rev. Mod. Phys. **88**, 045006 (2016).

[38] J. W. Cannon, J. A. Aronovitz, and P. Goldbart, J. Phys. I **1**, 629 (1991).
[39] M. Bernabei, P. Bacova, A. J. Moreno, A. Narros, and C. N. Likos, Soft Matter **9**, 1287 (2013).
[40] J. Elgeti and G. Gompper, Europhys. Lett. **101**, 48003 (2013).
[41] I. D. Vladescu, E. J. Marsden, J. Schwarz-Linek, V. A. Martinez, J. Arlt, A. N. Morozov, D. Marenduzzo, M. E. Cates, and W. C. K. Poon, Phys. Rev. Lett. **113**, 268101 (2014).
[42] T. S. van Erp, D. Moroni, and P. G. Bolhuis, J. Chem. Phys. **118**, 7762 (2003).
[43] R. J. Allen, C. Valeriani, and P. R. ten Wolde, J. Phys. Condens. Matter **21**, 463102 (2009).
[44] R. Fettiplace and D. A. Haydon, Physiol. Rev. **60**, 510 (1980).
[45] Y. Fily, A. Baskaran, and M. F. Hagan, arXiv:1601.00324.
[46] The system of Fily *et al.* [45] corresponds to a limit of our system in which the persistent length v_0/D_t is much larger than both radii of curvature. Noting that at the apices of our system $H^2 = G$, the accumulation of particles at the region of high Gaussian curvature G as observed by Fily *et al.* is consistent with the superlinear increases of the pressure with curvature as reported here.
[47] Y. Fily and M. C. Marchetti, Phys. Rev. Lett. **108**, 235702 (2012).
[48] L. Rayleigh, London Edinburgh Dublin Philos. Mag. J. Sci. **34**, 145 (1892).
[49] L. A. Cameron, P. A. Giardini, F. S. Soo, and J. A. Theriot, Nat. Rev. Mol. Cell Biol. **1**, 110 (2000).
[50] E. W. Burkholder and J. F. Brady, Soft Matter **14**, 3581 (2018).
[51] S. Thutupalli, D. Geyer, R. Singh, R. Adhikari, and H. A. Stone, Proc. Natl. Acad. Sci. U.S.A. **115**, 5403 (2018).